Mechanical Behavior of T-shaped Concrete-filled steel tubular Columns Subjected to Concentric and Eccentric Compressive Loads

Yuanlong Yang [1], Yuyin Wang [2,*], Feng Fu [3]Liu J

(1. Key Laboratory of Mechanics on Disaster and Environment in Western China of China Ministry of Education, Lanzhou University, Lanzhou 730000, China;

2. School of Civil Engineering, Harbin Institute of Technology, Harbin 150090, China)

3. School of Engineering and Mathematical Sciences, City University London, Northampton Square, EC1V 0HB London, UK

Abstract: In this paper, a batch of T-shaped concrete-filled steel tubular (CFST) columns, T-shaped steel tube confined concrete (STCC) columns and T-shaped reinforced concrete (RC) counterparts were tested under both concentric compressive load and eccentric compressive load. The battlement-shaped bar and tensile bar stiffeners were developed to delay local buckling in tube wall. The mechanism of the stiffening, the failure modes of concrete and steel tubes, the strength and ductility of specimens were investigated in detail during the experimental research. A numerical modeling program was developed and verified against the experimental data. The numerical program, which incorporates the effect of the stiffeners on postponing local buckling of the tube and the confinement of the tube on concrete core, was used to carry out comprehensive parametric analysis , therefore, finding the influencing factors on the mechanical behavior of T-shaped CFST columns.

Keywords: concrete-filled steel tubular column; T-shape; concentric compressive load; eccentric compressive load; stiffener

1. Introduction

Rectangular cross-sectional columns in traditional frame structures (as it shows in Figure 1), with extended corners to indoor space, normally have larger sectiondepths than those of adjoining infilled walls, leading to reduction of usable indoor space and disturbance to indoor environment. Recently, special-shaped cross-sectional columns, as an improved architectural approach, have been increasingly introduced into residential and official buildings. Smooth connection of special-shaped columns and adjacent infilled walls guarantees increased efficiency of indoor space and availability to furniture setting out (in Figure 2).

Systematic research and extensive engineering practice have been carried out on RC special-shaped column. Early study mainly focused on the static behavior of T-shaped and L-shaped stub columns subjected to concentric compressive load or biaxial eccentric compressive load, based

*Corresponding author

Tel: +86 451 8628 2079; Fax: +86 451 8628 2083

on which, interaction curve of resistances for practice was proposed (Joaquin, 1979; Cheng and Hsu, 1989; Mallikarjuna and Mahadevappa, 1992; Dundar and Sahin, 1993; Yau *et al*., 1993). Since 2000, to comply with development of housing industry, extensive study carried by Chinese researchers (Zhang and Ye, 2003; Gao *et al*., 2005; Wang *et al*., 2007) has concentrated on comprehensive static and seismic behaviors, especially for RC special-shaped columns in structural systems.

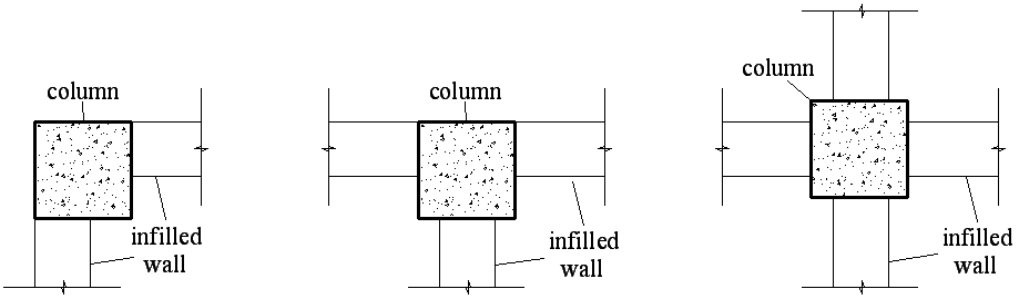

Figure 1. Rectangular cross-sectional columns in frame structure

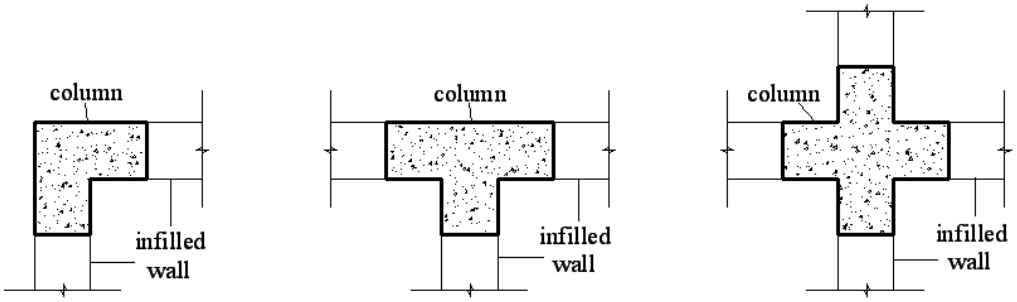

Figure 2. Special-shaped cross-sectional columns in frame structure

The irregularity in cross section of special-shaped column brings disadvantages in its mechanical behavior, and leads to strict limitations in aseismic design: the RC special-shaped columns can only be used to 8-degree seismic fortification zone (0.2g) or below; its applicable maximum building height is rigorously restricted, compared with that of rectangular RC columns (listed in Table 1), based on the Chinese codes - Technical specification for concrete structures with specially shaped columns (JGJ 149-2006/JGJ 514-2006) and Code for design of concrete structures (GB 50010-2010).

Table1. Maximum building height of special-shaped and rectangular columns in frame structures (unit: m)

Section	Non-seismatic design	Aseismic design					
		6-degree	7-degree		8-degree		9-degree
		0.05g	0.1g	0.15g	0.2g	0.3g	0.4g
Special shape	24	24	21	18	12	—	—
Rectangular shape	70	60	55	55	45	45	25

To improve the dynamic behavior of special-shaped columns, research and promotion of special-shaped CFST columns have been in the ascendant. Recent research mainly focused on local buckling delay of steel tubes and mechanical behavior of stiffened special-shaped CFST columns. The plate rib, which is the most commonly used stiffener in square CFST column, has been introduced into the L-shaped CFST columns (Shen and Chen, 2003). The plate ribs reinforce the tube by enlarging bending rigidity of steel plate sections. An experiment on this kind of member in

frame structures was carried out to investigate its seismic behavior (Zhang and Shen, 2010). Pulled binding bars were adopted at possible plastic hinge locations in the T-shaped and L-shaped CFST columns. Experimental and theoretical research has been conducted subjected to concentric and eccentric loads to study their static behavior (Zuo and Cai, 2012a; Zuo and Cai, 2012b). A latticed special-shaped column composed of concrete filled steel tubes was experimented subjected to a constant axial load and a cyclical flexural load (Zhou and Chen, 2012). This kind of column worked together well and the seismic behavior of SCFST columns was good.

An experiment of T-shaped CFST columns subjected to concentric compressive load or eccentric compressive load is presented in this paper. Battlement-shaped bar and tensile bar stiffeners were introduced in CFST specimens to postpone tubes' local buckling. Failure modes and static mechanical properties of the specimens were investigated. Theoretical analysis, with numerical program verified by experimental results, was carried out parametric study, trying to find influence factors. simplified model to predict resistance, based on experimental and theoretical analysis, was proposed for actual practice.

2. Experimental study

2.1 Details of the specimens

Basic information of The specimens in this experiment, is summarized in Table 2, consist of 7 concentrically loaded specimens (TA group) and 4 eccentrically loaded specimens (TE group). In the TA group, the stiffening mechanism and the constraint effect for concrete provided by steel tube are key factors to be studied TA1 is RC counterpart(I presume) specimen, designed referred to China code "Technical specification for concrete structures with specially shaped columns (JGJ 149-2006)"; TA2 is non-stiffened CFST specimen; TA3 and TA4 are battlement-shaped bar stiffened CFST specimens; TA5 is tensile bar stiffened CFST specimen; TA6 is non-stiffened steel tube confined concrete specimen; TA7 is tensile bar stiffened steel tube confined concrete specimen. In the TE group, the parameter of eccentricity *e* was investigated except for specimen type. TE1 is RC referential specimen with eccentricity of 50mm; TE2 is non-stiffened CFST specimen with eccentricity of 50mm; TE3 is tensile bar stiffened CFST specimen with eccentricity of 25mm; TE4 is tensile bar stiffened CFST specimen with eccentricity of 50mm. The location of eccentric load is in the symmetric axis of cross section and offset from physical centroid toward the web.

Table2. Parameters of specimens

Group	Specimen	Specimen type	Stiffener type	Axial length *L* (mm)	Eccentricity *e* (mm)
TA	TA1	RC	—	900	0
	TA2	CFST	—	900	0
	TA3	Stiffened CFST	Battlement-shaped bar	900	0
	TA4	Stiffened CFST	Battlement-shaped bar	900	0
	TA5	Stiffened CFST	Tensile bar	900	0
	TA6	STCC	—	900	0
	TA7	Stiffened STCC	Tensile bar	900	0
TE	TE1	RC	—	1500	50

TE2	CFST	—	1500	50
TE3	Stiffened CFST	Tensile bar	1500	25
TE4	Stiffened CFST	Tensile bar	1500	50

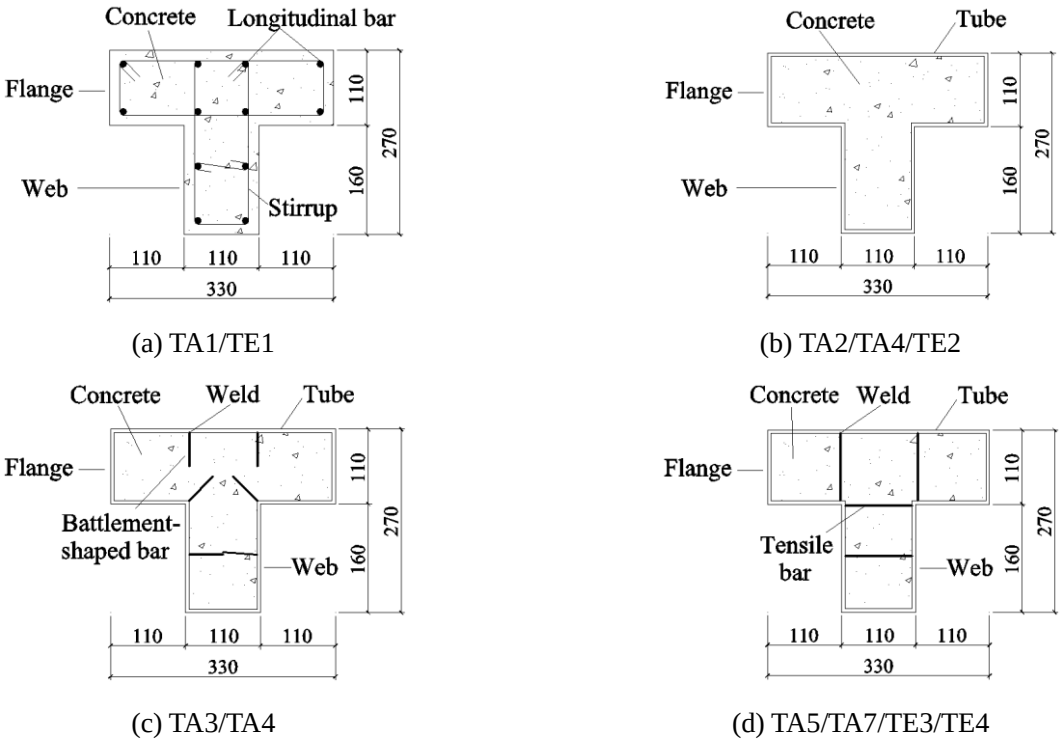

(a) TA1/TE1 (b) TA2/TA4/TE2

(c) TA3/TA4 (d) TA5/TA7/TE3/TE4

Figure 3. Cross-sectional dimensions of specimens

Restricted by instrumentation such as loading device and measuring apparatus, specimens were designed with similarity ratio of 1:2. The length L of axially loaded specimens and eccentrically loaded specimens are respectively 900mm and 1500mm. The cross sectional dimensions and constituents are demonstrated in Figure 3.

To postpone or restrain local buckling of T-shaped tubes, stiffeners using tensile bars were welded on the internal tube surfaces and concave corners, with longitudinal spacing of 100mm and with cross sectional distribution shown in Figure 3 (c). The tensile bar employs the straight hot-rolled plane bars. Holes, on the tube, with diameters slightly larger than those of the stiffeners, were drilled through allowing the stiffeners to pass through and to be welded at two ends.

During fabricating tubes in CFST specimens, steel plates were folded and welded into T-shaped cross-sectional hollow tube, followed by welding of an end plate on the bottom. For the stiffened specimens, tubes' welding was prior to the setting of tensile bars. This fabrication procedure reduced adverse influence caused by residual stress due to welding, comparing with traditional treatment. Ribs with the dimensions of 50mm×20mm×3.5mm, were welded at the end of the tubes to reinforce the tubes' end regions.

Layered concrete pouring process was adopted. The steel skeletons were put vertically for concrete to pour in and the concrete was vibrated with an electric vibrator until it was close-grained. During the 28-day's curing, top concrete was stricken off with high-strength cement mortar to

complement the shrinkage. For CFST specimens, another series of end-plates were welded to seal the top ends of the specimens.

2.2 Material properties

According to the Chinese National standard - Metallic materials-tensile testing at ambient temperature (GB/T 228-2002), mechanical properties of the steel plate and reinforcement bar were tested, and their material properties are collected in Table 2 and Table 3.

Table 2 Material mechanical properties of RC specimens

Specimen	Longitudinal bar		Stirrup		Concrete
	Yielding strength f_{lb} (N/mm^2)	Diameter d_{lb} (mm)	Yielding strength f_s (N/mm^2)	Diameter d_s (mm)	Prismatic compressive strength f_{ck} (N/mm^2)
TA1	353	12.1	373	6.5	23.2
TE1	353	12.1	373	6.5	37.5

Table 3 Material mechanical properties of CFST and STCC specimens

Specimen	Steel tube		Stiffener		Concrete
	Yielding strength f_y (N/mm^2)	Thickness t_y (mm)	Yielding strength f_{sr} (N/mm^2)	Diameter d_{sr} (mm)	Prismatic compressive strength f_{ck} (N/mm^2)
TA2	315	3.49	—	—	23.2
TA3	301	1.90	304	8.0	23.2
TA4	315	3.49	304	8.0	23.2
TA5	315	3.49	304	8.0	23.2
TA6	315	3.49	—	—	23.2
TA7	315	3.49	304	8.0	23.2
TE2	315	3.49	—	—	37.5
TE3	315	3.49	304	8.0	37.5
TE4	315	3.49	304	8.0	37.5

The concrete denoted C30 (according to a concrete code in China GB50010-2002), with the mix proportion shown in Table 4, was commercially ready-mixed and poured into hollow tubes, along with cubic standard test blocks in dimensions of 100mm×100mm×100mm. Test specimens' curing lasted to the day of trial and the cube blocks were tested to get the equivalent value of concrete compressive prismatic strength f_{ck} (in Table 2 and Table 3). on the test day, the axially loaded specimens is quite early compared with that of eccentrically loaded specimens, therefore its concrete prismatic strength (23.2MPa) is lower than the latter (37.5MPa). The corresponding cylinder strengths are respectively 27.2MPa and 44.8MPa.

Table 4 Mix proportions of concrete (kg/m^3)

Grade	Water	Portland cement	Sand	Gravel	Water reducing agent
C30	185	330	740	1030	8.6

2.3 Experimental devices and measuring apparatus

The experiment was carried out at the Structural and Seismic Test Research Center, Harbin Institute of Technology. A 500t computer OSD hydraulic pressure press was used as loading device, with two articulated rigid loading pads at the top and bottom, in which the bottom pad lifted the specimen and the top kept motionless.

In axially loaded specimen experiment, the axial load was measured with a load cell on the top end plate and a 20mm-thick padding plate was sandwiched between them in order to get evenly distributed axial loads, shown in Figure 4. Two accessary columns, on top of which are rigid elements of adjustable length, were specially designed to support the axial load along with the specimen, to stably get the load-displacement curves during load descending stage. Four displacement sensors were placed at bottom and two were at top, so effective vertical displacement u_r after the specimen and devises were close-contact, is calculated with Eq. (1):

$$u_r = u_b - u_t \tag{1}$$

Where

u_b is the average data value of the bottom four displacement sensors;

u_t is the average data value of the top two displacement sensors.

Four dial gauges were symmetrically arranged within 20mm initial gage length at mid-height of each steel plate (shown in Figure 4), for measuring displacement increment prior to local buckling and for physical centering adjustment before actual loading.

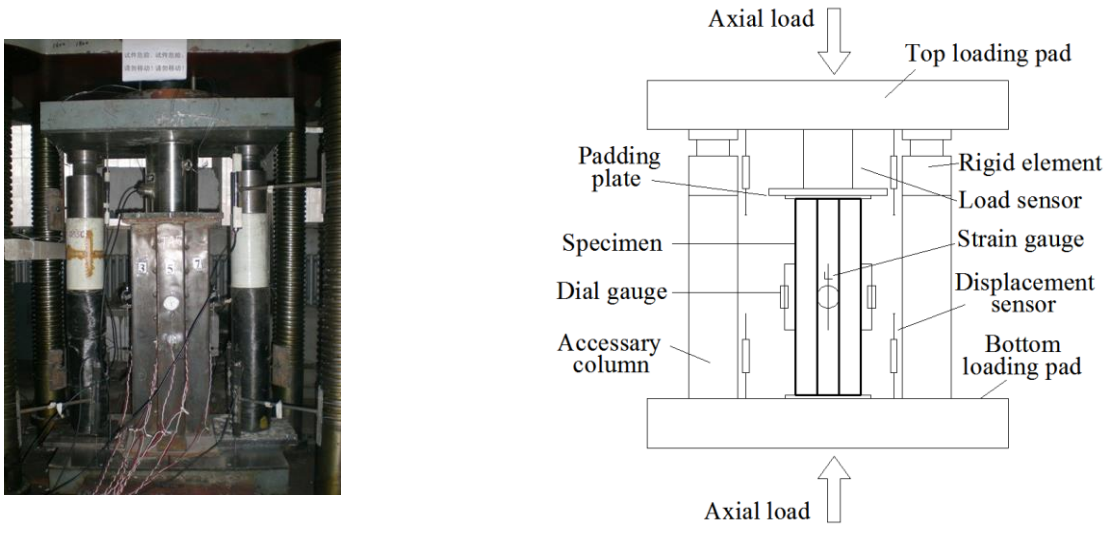

(a) Picture of loading (b) Illustrative drawing of loading

Figure 4. Loading devises and measuring apparatus in axial compressive experiment

In eccentrically loaded specimen experiment, a knife-edge articulation system was imbedded between loading pad and specimen, to simulate top and bottom articulated boundary conditions. The knife-edge articulation system consists of two close engaged parts: one rigid steel plate with a

centered triangular convex which is fixed on the loading pad and another rigid steel plate with saw-tooth triangular concaves fixed on the specimen. The magnitude of eccentricity is adjusted with different engaged location of triangular convex on the saw-tooth triangular concaves (shown in Figure 5).

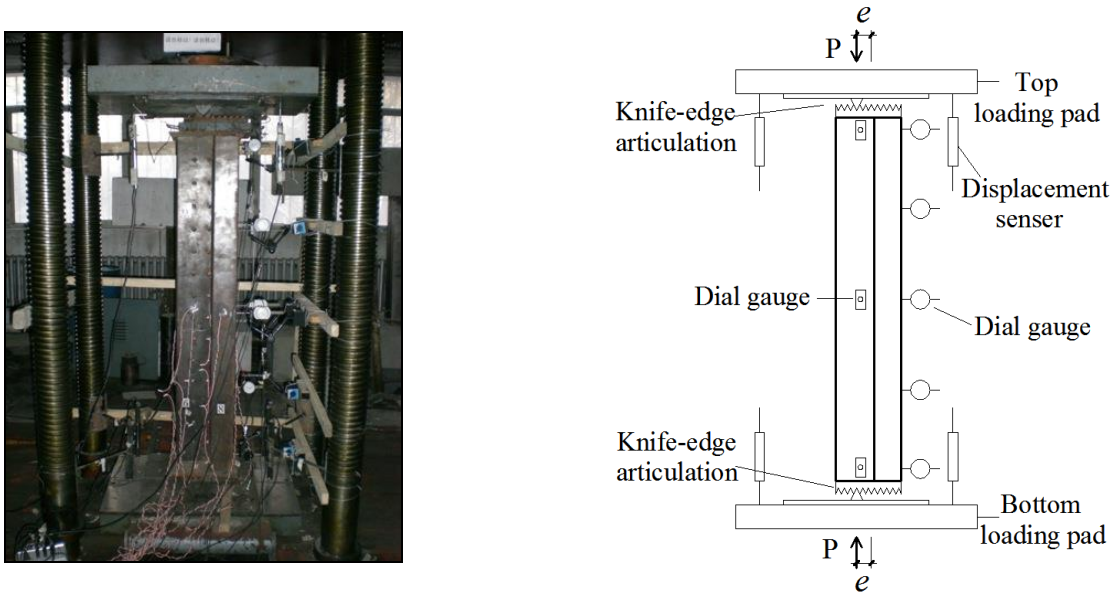

a) Picture of loading b) Illustrative drawing of loading

Figure 5. Loading devises and measuring apparatus in eccentric compressive test

The actual load was real-time monitored on the pressure press and recorded in every loading step. Same arrangement of displacement sensors with that in the axial experiment was adopted (shown in Figure 5). Five dial gauges were arranged in loading direction, quartering the specimen length, to measure its lateral displacement at different heights. Three dial gauges were arranged perpendicular to loading direction, to guarantee the specimen's unidirectional deformation.

2.4 Test phenomenon

2.4.1 Test phenomenon of specimens in TA group

During loading process, the macroscopic phenomenon was recorded to reasonably describe the mechanical behavior of the specimens, collaborated with the subsequent test data. The test phenomenon includes buckling behavior of steel tubes, concrete failure mode and interaction of concrete and steel tube.

2.4.1.1 Buckling behavior of steel tubes

Figure 6 illustrate the buckling modes of steel tubes of specimens TA2-TA7. The buckling formation time is denoted with load values or loading stages at the buckling positions of the steel tubes. The tube buckling is referred only to the cross-sectional buckling of the tube, where the buckling is only influenced by cross-sectional slenderness and in-filled concrete support. This is different to the end tube's buckling, which is caused by end concrete shrinkage resulting in the end tube bearing the axial load prior to the concrete core.

The specimens TA2, TA4 and TA5 can be compared together to investigate the role of stiffeners

in postponing local buckling of steel tubes. Due to absence of stiffeners' restraint, the steel tube of specimen TA2 separated from core concrete at the concave corner, which weakened boundary conditions of adjacent steel plates. The steel tube buckled at the ascending load of 2200kN. The maximum depth-to-thickness ratio (b/t =95) of steel plates of specimen TA2 is beyond the limits in Euro code 4 (EN1994-1-1: 2004) [14] in which the effects of local buckling can be neglected. Due to its flexible cross-sectional slenderness, the composite section of TA2 belongs to Class 4 grade according to the rules of cross-section classification in Euro code 4. Although the stiffened specimens TA4 and TA5 have the same depth-to-thickness ratio with specimen TA2, their local buckling was postponed to the load descending stage by battlement-shaped bar or tensile bar stiffeners. They finally failed by material failure beyond peak resistance, rather than local buckling failure in elastic and plastic stage. It can be indicated that, without thickening the tubes, the stiffeners help to increase the buckling resistance of columns, and further upgrade classification of composite sections to Class 2 grade in Euro code 4, in which the cross sections can develop their limited plastic resistances and deformation.

The specimens TA3 and TA4 can be compared to investigate the influence of tube thickness t, in other words, depth-to-thickness ratio b/t. Although stiffened by battlement-shaped bar, the specimen TA3 buckled locally at the load of 800kN due to its larger depth-to-thickness ratio (b/t=174). For specimen TA4 with the same stiffening scheme, by thickening the tube, no local buckling was detected until the load descending stage. It can be indicated that, thicker steel tube brings higher buckling resistance and upgrades classification of composite sections from Class 4 grade to Class 2 grade. However, in terms of material efficiency of steel tube, stiffener employment is more efficient than to thickness increase.

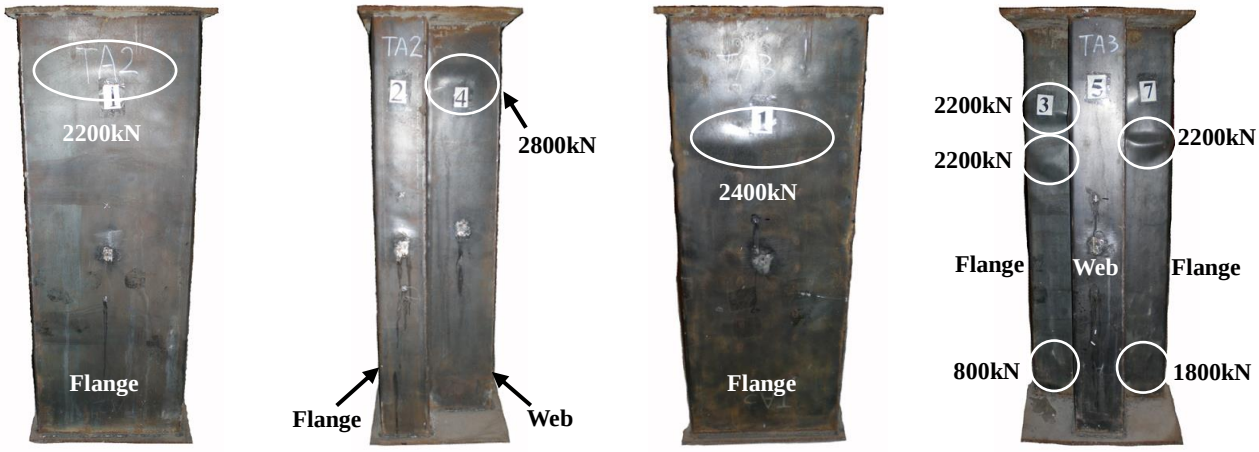

(a) TA2 (b) TA2 (c) TA3 (d) TA3

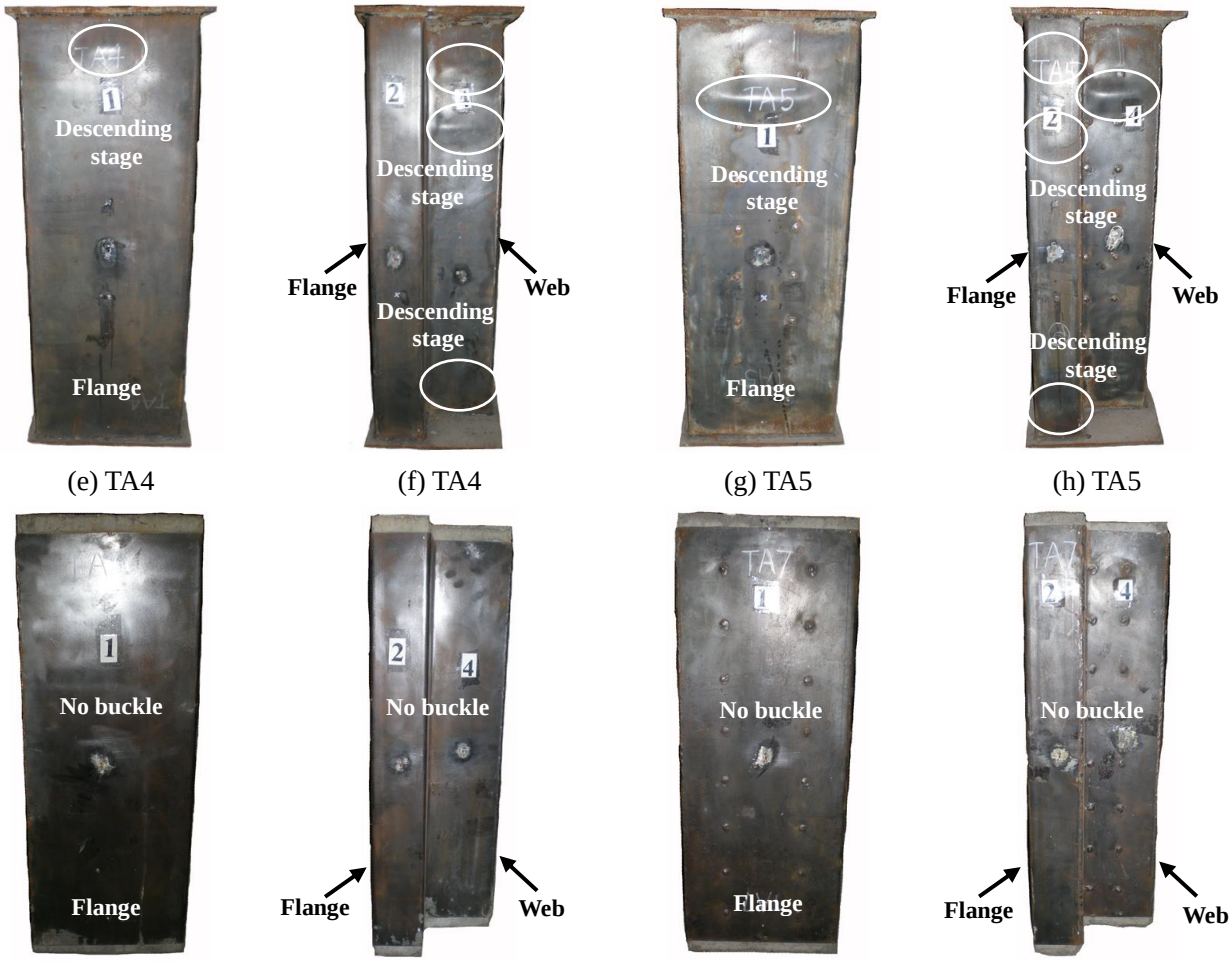

(e) TA4 (f) TA4 (g) TA5 (h) TA5

TA6 TA6 TA7 TA7

Figure 6. Buckling mode of steel tubes

The steel tube confined concrete specimens TA6 and TA7 can be compared to investigate the stiffeners in steel tubes with small vertical stress state. Because the steel tubes bear no vertical load directly, no local buckling was detected during the whole loading procedure for the two specimens. This phenomenon in the buckling behavior of steel tubes cannot guarantee that the in-filled concrete has the same mechanical behavior for the two specimens, which can be revealed in the following sectiont.

2.4.1.2 Stiffener behavior and concrete failure mode

The failure mode of RC specimen TA1 is concrete crushing. The crushed region was mainly located at the top half, and the concrete was seriously crushed in the web more than the flange, exposing the longitudinal bars and hoops near the crushed region (shown in Figure 7 (a)).

The cracks in concrete propagated rapidly but the concrete finally failed without obvious crushed mode. This type of failure mode cannot guarantee complete exploration of concrete compressive strength (shown in Figure 7 (b)).

The tensile bars in specimen TA5 increased interaction between concrete and steel tube and improved the concrete failure mode. After volume expansion of concrete overcomes that of the steel tube during loading, the tensile bar is well stretched to restrict the out-of-plane deformation at welds,

without any adverse mechanical impact on the concrete. in addition, the steel tube, strengthened by tensile bars, interacts well with core concrete at the concave corners and provides considerable confinement for core concrete. The concrete was compressed to serious crush and good exploration of concrete compressive strength was acquired (shown in Figure 7 (d)).

Adverse impact of separation between concrete and steel tube at concave corners was more serious especially when the tube breaks at ends in the specimen TA6 (shown in Figure 7 (e)). Bearing no axial load for the steel tube leads to two opposite mechanical effects: no buckle in steel tube and concrete's bearing axial load on its own. The former is favorable effect, but the latter adverse effect leads concrete ruptured and split into two parts suddenly, without any warning appearance (shown in Figure 7 (f)).

By arranging stiffeners at concave corners in specimen TA7, the interaction between concrete and steel tube was strengthened and the failure mode of concrete was greatly improved. Only several microcracks appeared in the flange and web, rather than complete rupture in specimen TA6 (shown in Figure 7 (g) (h)). Experimental phenomenon comparison of TA6 and TA7 deduced that the concave corners should be restricted with stiffeners, to avoid concrete premature brittle failure.

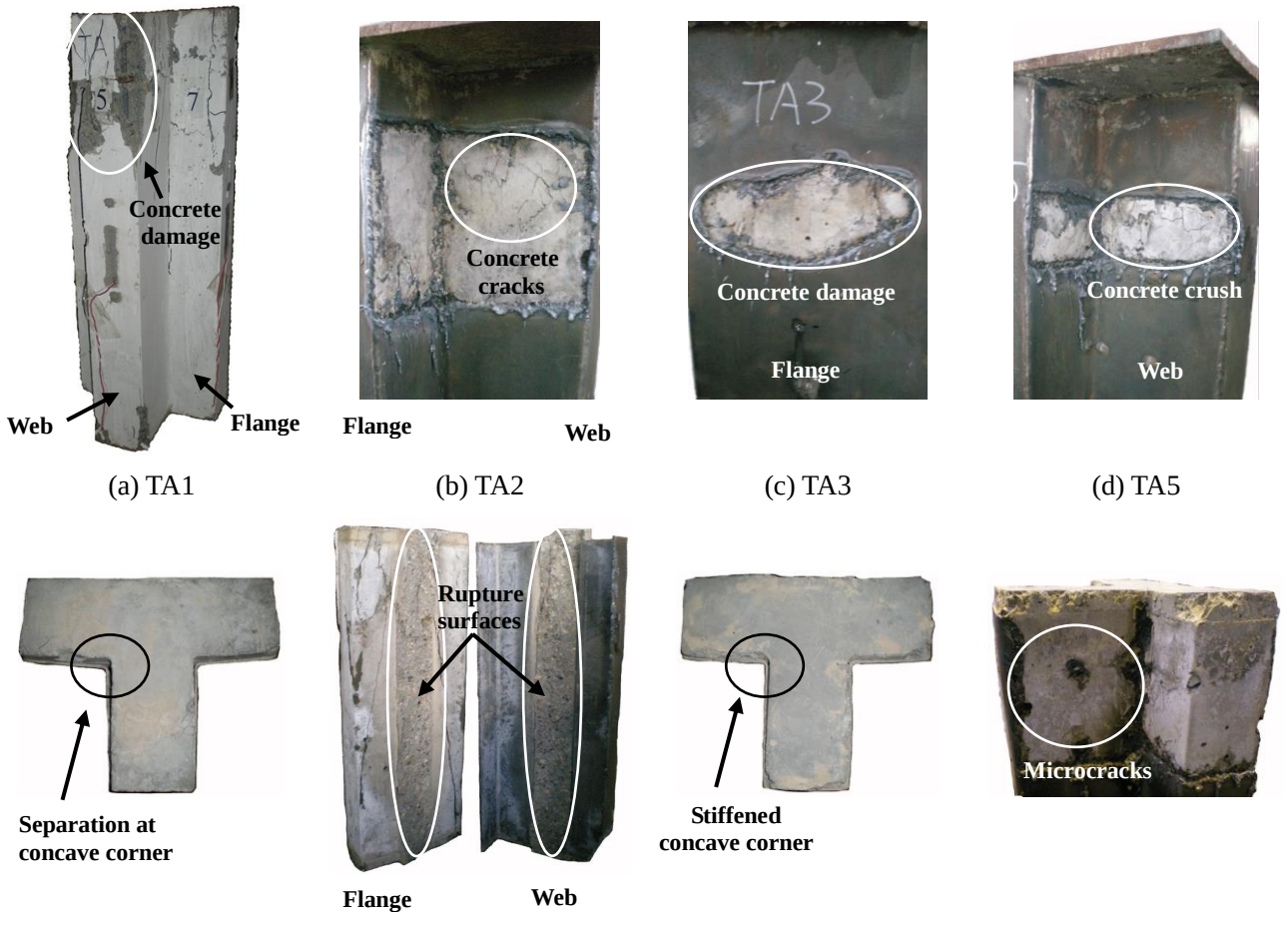

Figure 7. Concrete failure mode and interaction between concrete and steel tube

2.4.2 Test phenomenon of specimens in TE group

The failure mode of specimens in TE group is mainly mid-span bending failure, where the

curvature of deformed axis was larger than any other region due to articulated boundary conditions. Depending on off-center direction of vertical load and boundary conditions in TE group, the failure mode of cross sections in CFST specimens embodied steel plate buckling near midspan of specimens. The steel plates, far away from section center or with large depth-to-thickness ratio in compressive web region, buckled at ascending stage and further developed severely during descending stage (shown in Figure 8).

To RC specimen TE1, the web was crushed more severely than the flange. Diagonal cracks were observed in the web, and propagated to the web margin and the concave corner, resulting in concrete spalling in web margin and vertical cracks in concave corners (shown in Figure 8 (a) (d)).

Compared with RC specimen TE1, the concrete failure mode was improved and the confinement provided by steel tube played a certain role in non-stiffened CFST specimen TE2, but the interaction between steel tube and core concrete is still insufficient. After removing the steel tube, only local concrete in compressive region was crushed to brittle damage (superficial spalling and a few cracks in concave corner), which revealed the concrete compressive strength was inadequately utilized, especially after steel tube's premature local buckling. The crushed concrete expansion failed to overcome out-of-plane deformation of the tube, resulting in separation between concrete and tube at buckle positions and even at concave corners. (shown in Figure 8 (b) (e)).

The stiffened specimens TE3 and TE4 have similar failure mode. Taking the TE3 for example, the concrete was damaged in local crushed mode more seriously than that in non-stiffened specimen, i.e. large-area serious cracks. The crushed concrete was located between two adjacent stiffener welds, while concrete at welds showed less damage, for stiffeners restrain the neighboring steel tube to provide effective confinement for concrete. Little separation between concrete and tube was detected and their good interaction increased the exploration of material strength (shown in Figure 8 (c) (f)).

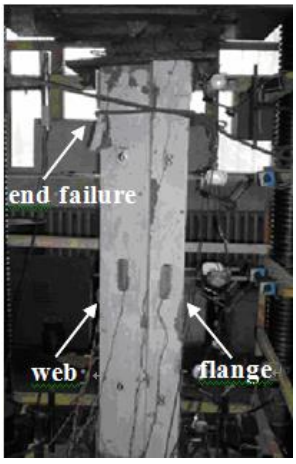

(a) TE1

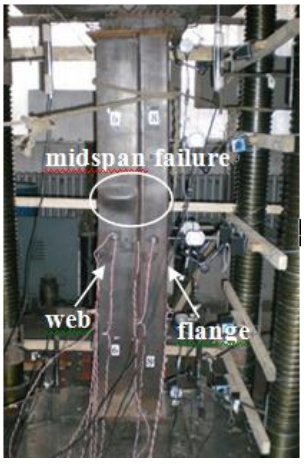

(b) TE2

(c) TE3

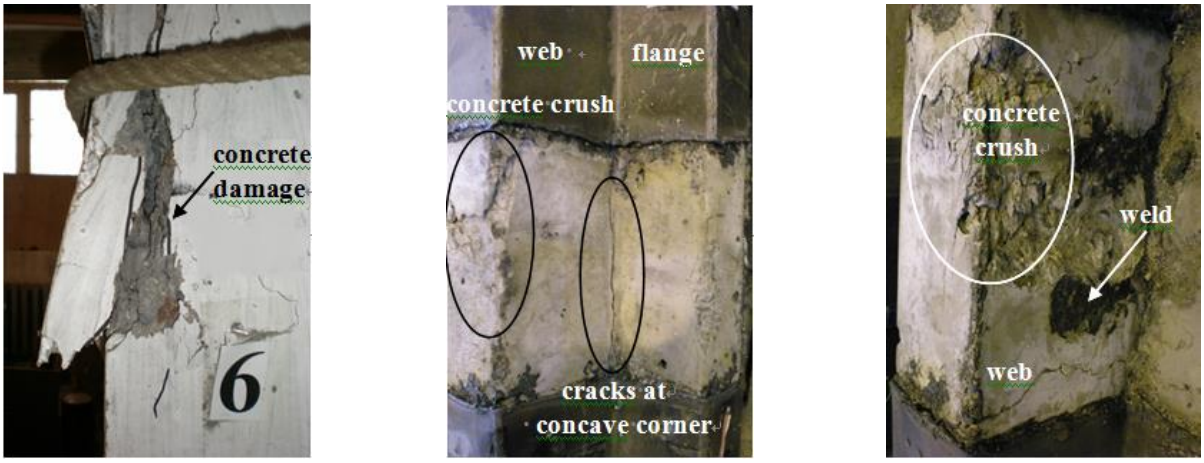

(d) TE1 (e) TE2 (f) TE3

Figure 8. Test phenomenon of specimens in TE group

3. Analysis of experimental results

3.1 Experimental results of specimens in TA group

Axial load-shortening relationship curves of specimens subjected to axial load are recorded in the experiment and compared in two groups in Figure 9. Primary mechanical properties calculated based on the relationship curves are listed in the Table 5, and some of mechanical properties are additionally explained in the following.

There are three featuring points on the relationship curves: the yielding point (U_y, P_y), the peak point (U_p, P_p) and the ultimate point (U_u, P_u). The yielding point is at the end of elastic stage and its corresponding shortening U_y and resistance P_y are calculated with specifications in China Standard "Specificating of Testing Methods for Earthquake Resistant Building (JGJ 101-96)"; the peak point is the point with the highest resistance; the ultimate point is the point with 85% of peak resistance during descending stage. In addition, the ductility factor μ is defined as the ratio of the ultimate shortening U_u to yielding shortening U_y:

$$\mu=U_u/U_y \tag{2}$$

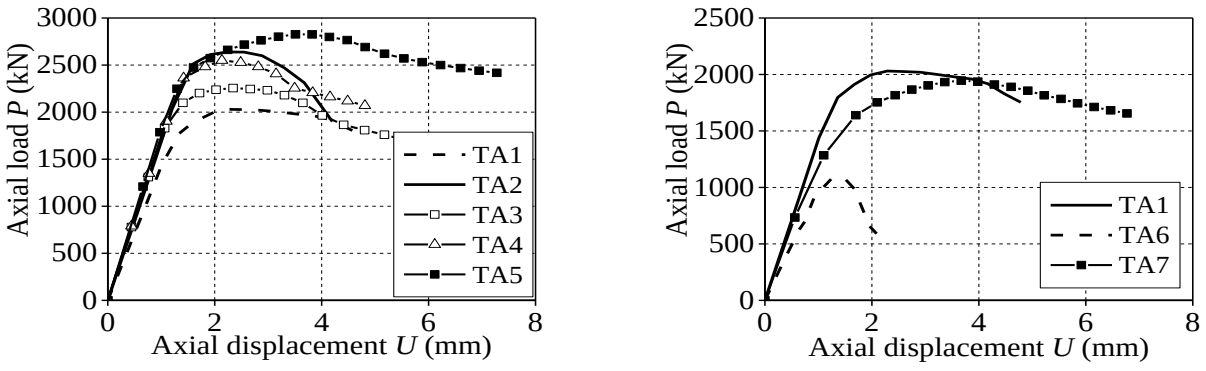

(a) (b)

Figure 9 Axial load-shortening curves

Table 5 Mechanical properties of specimens in TA group

Specimen	Peak resistance P_P(kN)	Resistance Enhancement $E_{P1}= P_P/ P_{TA1}$	Resistance Enhancement $E_{P2}= P_P/ P_{TA2}$	Ductility factor μ	Ductility enhancement $E_{\mu 1}=\mu/\mu_{TA1}$	Ductility enhancement $E_{\mu 2}=\mu/\mu_{TA2}$
TA1	2030	1.00	—	3.06	1.00	—
TA2	2672	1.32	1.00	2.19	0.72	1.00
TA3	2259	1.11	—	2.95	0.96	1.35
TA4	2549	1.26	0.95	2.66	0.87	1.21
TA5	2827	1.39	1.06	4.22	1.38	1.93
TA6	1094	0.54	—	1.41	0.46	0.64
TA7	1946	0.96	—	3.65	1.19	1.67

Figure 9 (a) illustrates that the CFST specimens TA2, TA3, TA4 and TA5 have obvious advantage on the axial compressive behavior over the RC specimen TA1. The peak resistances of CFST specimens are substantially increased due to steel tube and itd confinement on concrete. The specimen TA3 with lower steel ratio has the 11% enhancement ratio of ultimate resistance; the specimens TA2, TA4 and TA5 with higher steel ratio have 26%-39% enhancement, in which the specimen TA5 has the highest ultimate resistance. Compared with non-stiffened specimen TA2, the tensile bar stiffened specimen TA5 presents an increase of 6% in peak resistance, however the battlement-shaped bar stiffened specimen TA4 has a decrease of 5%. The stiffeners present positive function in improving specimen ductility. The battlement-shaped bar and tensile bar increase the ductility by 21% and 93% respectively compared with non-stiffened specimen. However the ductility of specimen TA4 is still lower than RC specimen TA1 by 13%. And meanwhile, the ductility of specimen TA5 is larger than RC specimen TA1 by 38%.

The tubes of specimens TA6 and TA7 break at two ends and bear no direct axial compressive load, to eliminate the disadvantage of steel tube buckling. For specimen TA7, the constraint effect from tensile bar stiffened steel tube approach its resistance to that of RC specimen TA1. And moreover, the tensile bar makes concrete resistance decrease more slowly and improved its ductility by 19% (shown in Figure 9 (b)). However, this mechanical behavior will not be anticipated if the concave corners fail to be restrained, such as in specimen TA6. Separation between concrete and steel tube can be detected at concave corners which makes longitudinal cracks propagate rapidly. Therefore exhibits less resistance and ductility of specimen TA6 than those of RC specimen TA1.

Based on the test data analysis, the tensile bar stiffener has proper mechanical behavior and the tensile bar stiffened specimen TA5 is provided with outstanding enhancement of peak resistance and ductility. For T-shaped tube confined concrete specimen, stiffeners are suggested to be placed at the concave corners of the T-shaped tube.

3.2 Experimental results of specimens in TE group

The mechanical properties of specimens in TE group have the same definition with those of specimens in TA group, except that the axial load-shortening curve is replaced by vertical

load-midspan horizontal displacement curve. Combining the experimental phenomenon with the mechanical properties, the mechanical behavior of specimens in TE group was investigated and analyzed in the Figure 10 and Table 6.

The confinement provided for concrete by steel tube is generally larger than that provided by stirrups. Although no obvious increase in ultimate resistance of CFST specimen TE2 was obtained compared with RC specimen TE1, the confinement for concrete began to work gradually during load descending stage and brought a ductility increase by 59%. To specimen TE4, the tensile bars further stiffened the steel tube and accordingly improved the confinement for concrete, which brought an increase in the peak resistance by 22% and ductility factor by 129% compared with specimen TE1.

For stiffened CFST specimens TE3 and TE4, with the eccentricity increasing, the TE4 has decreases in the peak resistance by 18% and ductility factor by 32%. Eccentricity's impact can be explained with sectional stress distribution. Due to second-order effect, with the eccentricity increasing, the mid-span normal stress distribution was transformed from total compression to partial compression and partial tension, which reduces the elastic stiffness, elastic-plastic stiffness, peak resistance and ductility.

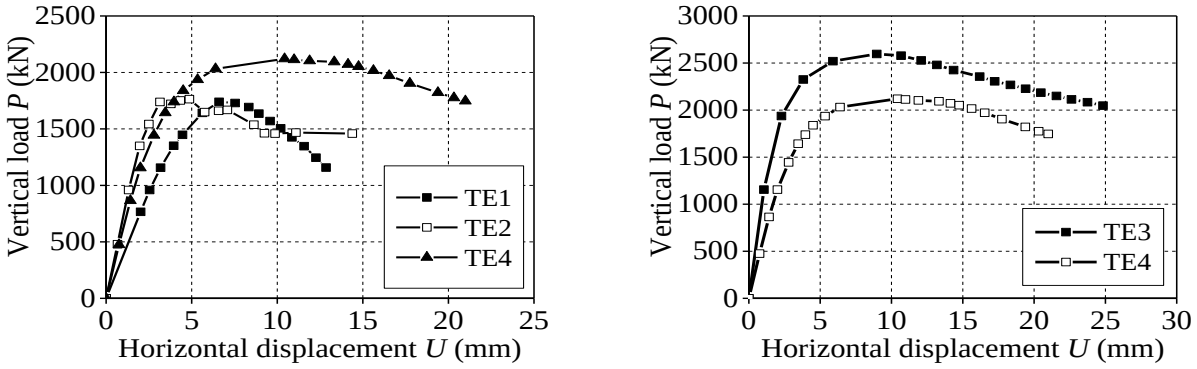

Figure 10 Comparison of vertical load-horizontal displacement curves of specimens

Table 6 Mechanical properties of specimens in TE group

Specimen	Peak resistance P_p(kN)	Resistance enhancement $E_p = P_p / P_{TE1}$	Ductility factor μ	Ductility enhancement $E_\mu = \mu/\mu_{TE1}$
TE1	1740	1.00	1.95	1.00
TE2	1739	1.00	3.10	1.59
TE3	2597	1.49	6.59	3.38
TE4	2120	1.22	4.46	2.29

4. Numerical analysis

4.1 Theory of numerical program

4.4.1 Numerical program of axially loaded T-shaped CFST columns

Based on the length range of experimental specimens, the numerical program is developed which aim to analyze T-shaped CFST stubs. The bending deformation, shear deformation, second-order effect are not included in the numerical program. Only axial deformation is taken into consideration and the strain distribution cross the section is considered as uniform in every cross section along column length. Axial displacement is applied on the top of the column and its bottom is fixed. The axial shortening of the column is then converted into sectional strain. The uniaxial constitutive relations of concrete and steel are employed to calculate axial stress, incorporating the effect of stiffeners on postponing tube's local buckling and the tube confinement for concrete core. The total resistance is summation of confined concrete and stiffened steel tube resistance.

Two numerical program is developed on is for eccentrically loaded columns and anther is for concentriclli loade columns (I presume)

4.1.2 Numerical program of eccentrically loaded T-shaped CFST columns

In numerical program of, axial and flexural deformation should be taken into consideration. Fiber-based model is employed in the following to carry out numerical analysis of the T-shaped CFST columns. Hypothesis of half sine wave is introduced to approximate column deformation. The internal axial force and bending moment are calculated on the cross section at the mid-span and iteration procedure is needed in seeking equilibration of internal and external forces. Due to material nonlinearity, geometric nonlinearity and cross-sectional nonsymmetry, seeking equilibration needs considering impact of torsional deformation of column.

The numerical analysis program adopts several following hypothesis: (1) During loading process the cross section always remains plane and no relative slip among steel tube and concrete is taken into consideration; (2) Take no account of the shear deformation; (3) In the analysis of simply supported member, the axial deformation is hypothesized as half sine wave; (4) Take no account of concrete tensile strength and consider concrete quitting work as soon as tensile strain emerges.

Numerical analysis program can be applied for T-shaped CFST cross section or member. The cross section analysis is the basis of overall member analysis. Both cross section and member analysis have three loading paths (in Figure 11): (I) vertical load N is applied prior to bending moment M while vertical load remaining unchanged; (II) Apply vertical load N while keeping load magnitude and load offset direction unchanged, that is to say, the bending moment M is proportional to the vertical load N; (III) bending moment M is applied prior to vertical load N and bending moment remaining unchanged, which is seldom in practical engineering. In numerical program of this paper, the loading path II was selected according to actual experimental loading scheme.

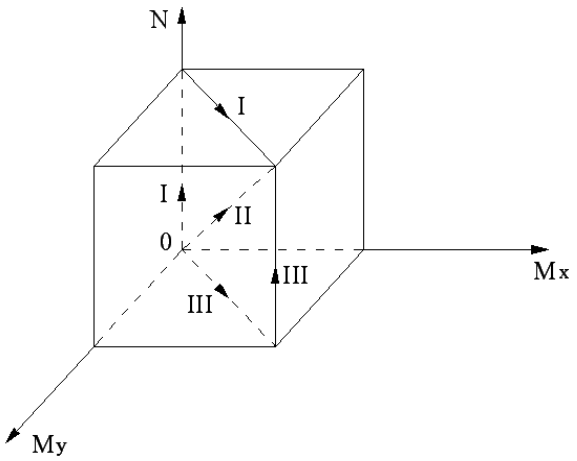

Figure 11. Loading paths of eccentrically loaded cross section and member

4.2 Uniaxial stress-strain relationship of materials

4.2.1 Uniaxial stress-strain relationship of confined concrete

(1) Confined concrete distribution

Compared to square CFST member, the T-shaped CFST member possesses more complex concrete confinement distribution, which is not only due to more edges and convex corners, but also due to two concave corners. The concave corners may produce problems on mechanical and deformable behavior for concrete and steel tube. The concrete confinement distribution for T-shaped CFST section is proposed in Figure 12(b), validated with some corresponding finite element analysis of T-shaped CFST columns. The confined concrete is marked with shaded area and the non-confined concrete is marked with blank areas. The central region of cross section is confined by outer concrete and belongs to confined concrete. Near convex corner of steel tube is confined concrete owing to sufficient stiffness. Near central region of each steel plate is non-confined concrete due to insufficient out-of-plane stiffness. Although with sufficient stiffness, near concave corner is non-confined concrete, due to separation between steel tube and concrete observed in the experiment. The boundary line between confined and non-confined regions is estimated with second-order parabola.

The employment of stiffeners can obviously change the concrete confinement distribution. Take the tensile bar stiffened CFST specimen for example. The tensile bars are welded at the steel plates with large depth-to-thickness ratio and at the concave corners. This stiffened scheme changes concrete confinement region distribution from Figure 12(b) to the shaded area in Figure 12 (d). The Figure 12 (d) illustrates concrete confinement region distribution of stiffened section 1-1 (shown in Figure 13) in which the tensile bar stiffeners are welded, therefore the stiffening effect for steel tube and confinement for concrete in section 1-1 are larger than those of any other section. The constraint point converts its neighboring previous non-confined region into confined region. Accordingly sectional non-confined region was decreased to smaller regions with constraint points as boundaries. It is worth noting that the concrete near concave corners are converted into confined region. The boundary line between confined and non-confined regions is still estimated with

second-order parabola.

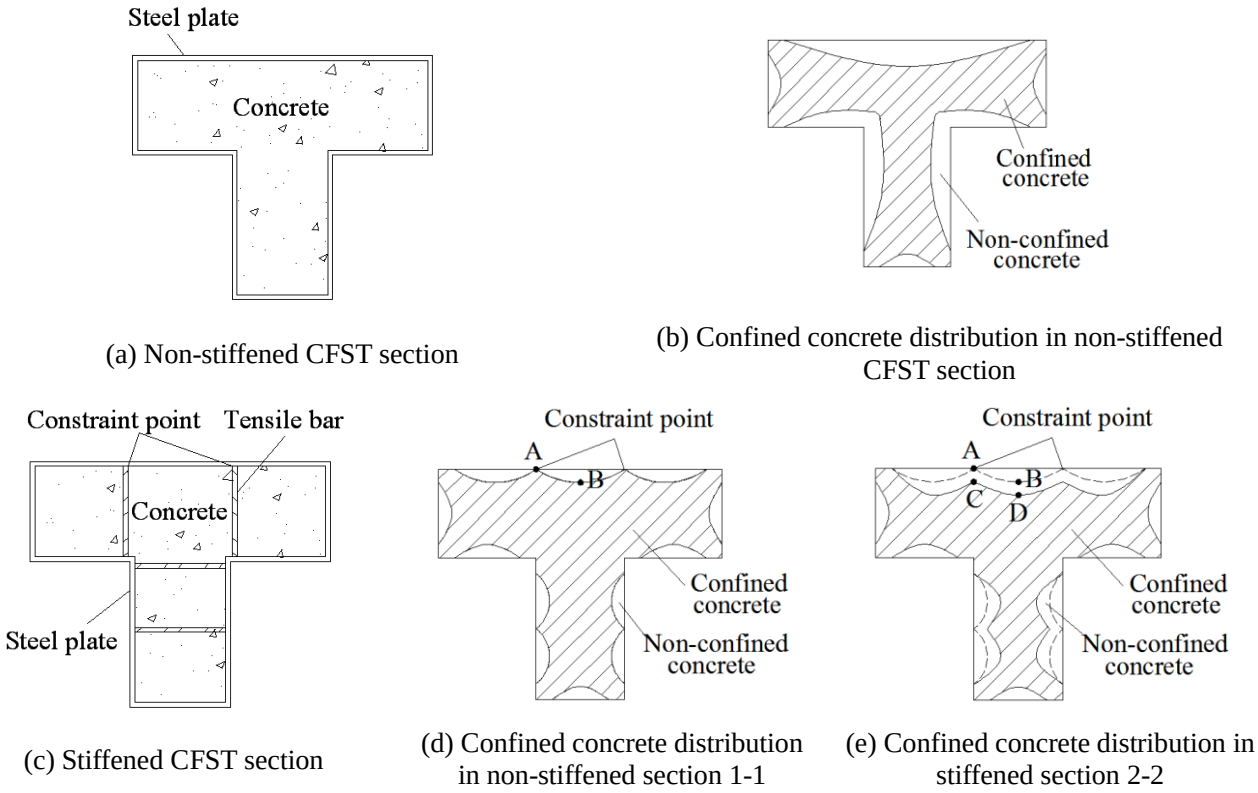

(a) Non-stiffened CFST section

(b) Confined concrete distribution in non-stiffened CFST section

(c) Stiffened CFST section

(d) Confined concrete distribution in non-stiffened section 1-1

(e) Confined concrete distribution in stiffened section 2-2

Figure 12 Cross-sectional confined concrete distribution of T-shaped CFST

The Figure 13 shows the longitudinal distribution of confined concrete. The 2-2 section, defined as non-stiffened section, is the middle section between two adjacent stiffened sections 1-1. The concrete confinement region distribution of section 2-2 is displayed with shaded area in Figure 12 (e), in which the dash line is the boundary of confined concrete in non-stiffened section 1-1. As demonstrated in Figure 13, the longitudinal boundary line (the solid line) of confined concrete (the shaded region) and non-confined concrete (the blank region) is still estimated with second-order parabola between two adjacent stiffened sections. The dash line in the Figure 13 is parallel to the solid longitudinal boundary line. The non-stiffened section 2-2 with the smallest confined region is the most likely damaged section, thus it directly determines member's mechanical behavior. The resistance of section 2-2 can be considered as the resistance of column.

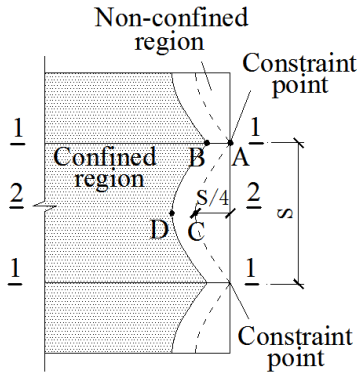

Figure 13 Longitudinal distribution of confined concrete

There are four characteristic points A, B, C and D on the sectional and longitudinal boundary

lines. Combined with Figure 12(e) and Figure 13, point A is constraint point of stiffener in the stiffened section; point B is the middle point of the sectional boundary line between two constraint points in the stiffened section; point C is corresponding point in the non-stiffened section which point A extends along longitudinal boundary line; point D is corresponding point in the non-stiffened section which point B extends along longitudinal boundary line. The confined concrete distribution is the basis of establishing numerical method to compute compressive strength of confined concrete.

(2) Lateral confining pressure of concrete

In the Mander model (Mander, 1988) for confined concrete, the lateral confining pressure is the main factor for axial compressive strength enhancement. The Mander model can be further modified and applied to the confined concrete of square CFST columns (Yang, 2014). However, for the T-shaped cross section CFST is more complex than square cross section CFST, the calculating method of lateral confining pressure of concrete in square CFST should be further modified for the T-shaped CFST. In Figure 14, the tensile bar stiffeners actually divide T-shaped section into several rectangular parts. The confined concrete distribution in each part is similar to that in rectangular CFST, except for the constraint region at the boundary of two adjacent rectangular parts, where the concrete is confined by outer concrete (shown in Figure 12 (d)) rather than steel plate. Based on the equilibrium of forces in cross section, within the vertical spacing range of two adjacent constraint points, it can be deduced in Figure 14 that the tensile force in bar a (in Figure 14) is approximately equal to the horizontal tensile force in plate C; the tensile force in bar b is approximately equal to that of the plate D; the tensile force of the bar c is approximately equal to that of the plate A and B. So the tensile bar can be equivalent to steel plate with the same thickness with steel tube.

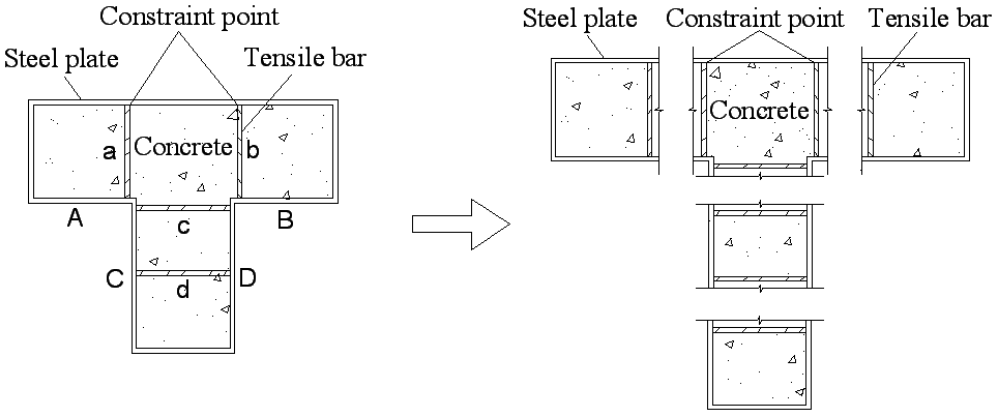

Figure 14 Cross-sectional simplification of T-shaped CFST

The tensile bar stiffeners transform the T-shaped CFST column to several equivalent rectangular CFST parts. Therefore the numerical method for square CFST column (Yang, 2014) can be further modified and employed to calculate the lateral confining pressure of concrete. It should be noted that steel plates with different depth-to-thickness ratios provide different lateral confining pressures for concrete. The lateral confining pressure from steel plate with large depth-to-thickness is less

than that from steel plate with small depth-to-thickness. The weighted mean lateral confining pressure for concrete in rectangular CFST section, therefore, lies between those provided by the two kinds of steel plates. In this numerical program, in order to get equivalent lateral confining pressure f_l for concrete in T-shaped CFST section, the lateral confining pressure f_{li} of the ith steel plate, which is calculated in rectangular CFST section, is averaged with its depth-to-thickness ratio D_i/t as weighted coefficient:

$$f_l = \frac{\sum_{i=1}^{m}(D_i / t) f_{li}}{\sum_{i=1}^{m}(D_i / t)} \tag{3}$$

Where m is number of all the steel plates in T-shaped tube.

With regard to the equivalent rectangular CFST column, the equilibrium diagram of sectional forces by considering the half body confined by a steel tube is shown in Figure 15. During peak resistance, the transverse stress f_h of steel plate can be approximated as 10% of yielding strength f_y (Elremaily and Azizinamini, 2002). Specially for stiffened steel tube confined concrete specimen TA7 in this paper, the transverse stress f_h of steel plate is suggested as 20% of yielding strength f_y. If the transverse stress f_h of steel plate exerts a uniform lateral stress f_{li} on the concrete core, then equilibrium of forces per unit column length required that

$$2F_s = F_c \tag{4}$$

$$F_s = f_h t = 0.1 f_y t \tag{5}$$

$$F_c = f_{li} L_i \tag{6}$$

Where the F_s is transverse tensile force of steel plate; the L_i is cross-sectional dimension of concrete; the t is thickness of steel plate.

The lateral confining pressure f_{li} for concrete is then obtained based on equations (4), (5) and (6)

$$f_{li} = 0.2 f_y t / L_i \tag{7}$$

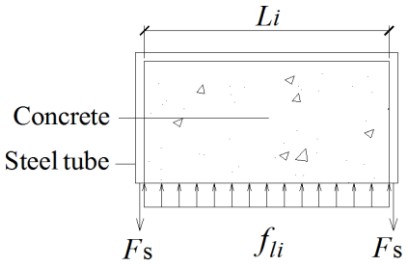

Figure 15 Equilibrium diagram of cross-sectional forces

(3) Compressive strength of confined concrete

The ratio of confined concrete area to total concrete area in section 2-2 is a key factor to determine the compressive strength of confined concrete. Firstly the non-confined concrete area in section 1-1 should be calculated. On the basis of previous finite element analysis, the concrete confinement distribution of stiffened section is presented in Figure 12 (d). Each non-confined region in 1-1 section is enveloped by a straight line and a second-order parabola curve with an angle

of 45 degrees on the steel plate. The area of each non-confined region is calculated as $W_i^2/6$, in which the W_i is the dimension of non-confined region at straight line boundary (shown in Figure 16, i=1-7). The characteristic dimensions at convex corners and concave corners are estimated as 1/6 of shorter intersecting plate length.

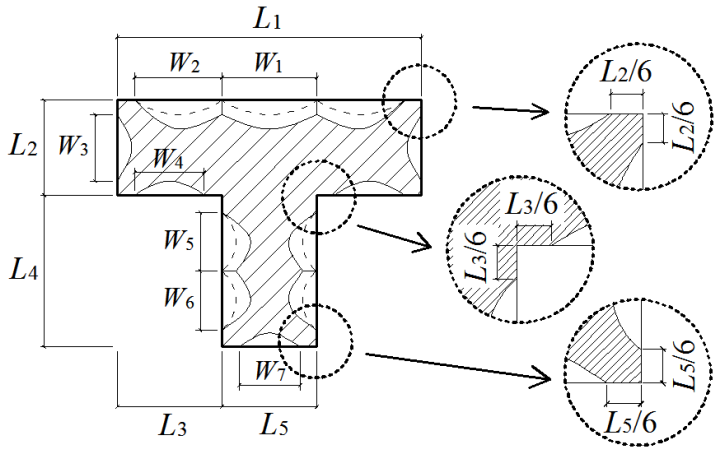

Figure 16 Confined concrete distribution in section 1-1 and 2-2 of T-shaped CFST

The characteristic dimension W_i of the *ith* non-confined region, defined in Figure 16, is calculated in the following formulas:

$$W_1 = L_1/3 - d_t \tag{8-a}$$

$$W_2 = L_1/3 - d_t/2 - (L_1/3)/6 \tag{8-b}$$

$$W_3 = L_2 - 2L_2/6 \tag{8-c}$$

$$W_4 = L_3 - 2L_3/6 \tag{8-d}$$

$$W_5 = L_4/2 - (L_4/2)/6 - d_t/2 \tag{8-e}$$

$$W_6 = L_4/2 - (L_4/2)/6 - d_t/2 \tag{8-f}$$

$$W_7 = L_5 - 2L_5/6 \tag{8-g}$$

Where d_t is the diameter of the bar stiffener (mm); L_i is the cross-sectional depth of the *ith* steel plate (mm).

In Figure 13, the longitudinal boundary line (the solid line) of confined concrete and non-confined concrete is estimated with second-order parabola, with an angle of 45 degrees on the steel plate. Each non-confined region area in the non-stiffened section 2-2 is obtained in the following formulas:

$$A_1 = \frac{2}{3}W_1(\frac{1}{4}W_1) + W_1(\frac{1}{4}S) = \frac{1}{6}W_1^2 + \frac{1}{4}W_1S \tag{9-a}$$

$$A_2 = \frac{2}{3}W_2(\frac{1}{4}W_2) + \frac{1}{3}W_2(\frac{1}{4}S) + \frac{1}{2}W_2(\frac{1}{4}S) = \frac{1}{6}W_2^2 + \frac{3}{24}W_2S \tag{9-b}$$

$$A_3 = \frac{2}{3}W_3(\frac{1}{4}W_3) = \frac{1}{6}W_3^2 \tag{9-c}$$

$$A_4 = \frac{2}{3}W_4(\frac{1}{4}W_4) = \frac{1}{6}W_4^2 \tag{9-d}$$

$$A_5 = \frac{2}{3}W_5(\frac{1}{4}W_5) + \frac{1}{3}W_5(\frac{1}{4}S) + \frac{1}{2}W_5(\frac{1}{4}S) = \frac{1}{6}W_5^2 + \frac{3}{24}W_5S \quad (9\text{-e})$$

$$A_6 = \frac{2}{3}W_6(\frac{1}{4}W_6) + \frac{1}{3}W_6(\frac{1}{4}S) + \frac{1}{2}W_6(\frac{1}{4}S) = \frac{1}{6}W_6^2 + \frac{3}{24}W_6S \quad (9\text{-f})$$

$$A_7 = \frac{2}{3}W_7(\frac{1}{4}W_7) = \frac{1}{6}W_7^2 \quad (9\text{-g})$$

The total non-confined region area A_{co} in the cross section 2-2 is the summation of all non-confined region area:

$$A_{co} = \sum_{i=1}^{n} A_i \quad (10)$$

Where A_i is the area of the *ith* non-confined region area (mm^2); *i* is the sequence number of non-confined region area; *n* is the number of non-confined regions.

The area of confined concrete in the non-stiffened section A_{cc} is

$$A_{cc} = A_c - A_{co} \quad (11)$$

The confinement effectiveness coefficient k_e is defined as

$$k_e = \frac{A_{cc}}{A_c} \quad (12)$$

The uniformly distributed lateral pressure $f_l^{'}$ in the control section is defined

$$f_l^{'} = k_e f_l \quad (13)$$

The uniformly distributed lateral pressure $f_l^{'}$ is used in the Mander concrete model to calculate the compressive strength of the confined concrete f_{cc}:

$$f_{cc} = f_{ck}(-7.333(f_l^{'} / f_{ck})^2 + 6.533(f_l^{'} / f_{ck}) + 1) \quad (14)$$

Since the concrete tensile strength is far less than the compressive strength, it can be neglected in the behavioral analysis and can be considered as zero in the numerical program.

4.2.2 Uniaxial stress-strain relationship of stiffened T-shaped tube

For the local buckling of steel plates in T-shaped CFSTs subjected to concentric compressive load, the elastic buckling strength $f_{cr}^{'}$ (N/mm^2) of stiffened steel plates can referred to formula (15), which is proposed in the author's another paper (Yang and Wang, 2014).

$$f_{cr}^{'} = \alpha_a \alpha_b \frac{\pi^2 D}{b^2}(4\frac{a^2}{b^2} + 4\frac{b^2}{a^2} + \frac{8}{3}) \quad (15)$$

For the steel plate with large depth-to-thickness ratio is prone to buckle than those with small depth-to-thickness ratio, the elastic buckling strength $f_{cr}^{'}$ can be applied for steel plates with depth-to-thickness ratio larger than $60\sqrt{235/f_y}$ and it should not exceeds yield strength f_y.

For the steel plates in T-shaped CFSTs subjected to eccentric compressive load, the numerical method to calculate elastic buckling strength $f_{cr}^{'}$ can be further developed to concentric compressive load scenarios . Firstly the stress distribution of steel plates subjected to concentric

compressive load N_s can be simplified as the diagram in Figure 17. The Figure 17 (b) shows the stress distribution corresponding to local buckling. Because out-of-plane buckling mainly lies in the central part of steel plate, the diagram in Figure 17 (b) can be transformed to simplified stress mode in Figure 17 (c). The central part with width of B_u is assumed to bear no load, while the two corner parts with width of $B_e/2$ reach yield strength f_y. To satisfy the force equilibrium, the areas of stress diagrams of Figure 17 (b) and (c) should be equal. Thus the dimension B_u can be calculated:

$$B_u = (1 - f_{cr}^{'} / f_y)B \tag{16}$$

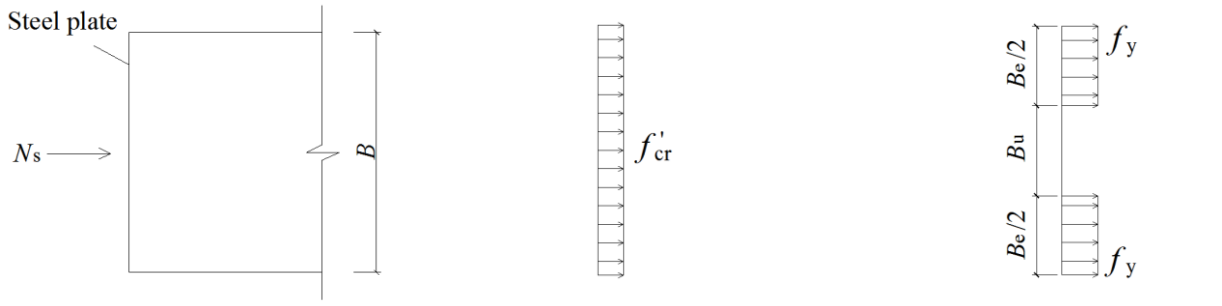

(a) Loading mode (b) Stress distribution at local buckling (c) Simplified stress mode

Figure 17 Stress distribution and its simplified mode of steel plate subjected to concentric load

Figure 18 is the stress distribution and its simplified mode of steel plate subjected to eccentric load. The eccentric load can be equivalent to concentric load N_s plus moment M (Figure 18 (a)). It is also assumed that local buckling can be considered in the numerical analysis if the depth-to-thickness ratio larger than $60\sqrt{235/f_y}$ and the elastic buckling strength $f_{cr}^{'}$ should not exceeds yield strength f_y. Figure 18 (b) respectively illustrates the four types of stress distributions close to occurrence of local buckling with the ratio of M to N_s increasing.

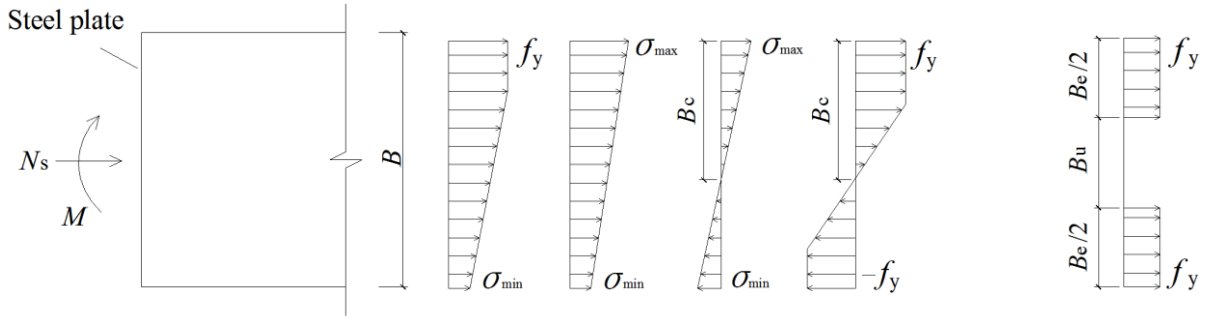

(a) Loading mode (b) Stress distribution at local buckling (c) Simplified stress mode

Figure 18 Stress distribution and its simplified mode of steel plate subjected to eccentric load

As for the steel plate with fully compressive cross section, the steel plate can be considered entering buckling if sectional stress satisfies the following condition:

$$\sum_{i=1}^{n} \sigma_i A_i = f_{cr}^{'} Bt \tag{17}$$

Where σ_i and A_i are stress and area of the *ith* element in cross section; t is the steel plate thickness; n is number of steel plate elements in cross section.

With regard to the steel plate with partially compressive cross section, if the width-to-thickness ratio of steel plate in compression exceeds $60\sqrt{235/f_y}$, steel plate's buckling can also be judged by equation (17).

As the simplified stress mode in Figure 17 (c) also applies to steel plates subjected to eccentric compressive load (Figure 18 (c)), Thus the dimension B_u can still be calculated with formula (16) to satisfy the force equilibrium. It is specially explained that for steel plate with partially compressive cross section, the B in formula (16) should be replaced by compressive dimension B_c.

In the Numerical program, the resistance of steel tube is superposition of those of all the steel plates. The simplified stress mode in Figure 17 (c) is used as the stress distribution of steel plate after local buckling occurrence and remains unchanged during the following loading. For tensile bar stiffened steel tube confined concrete specimen TA7, only confined concrete is considered in the calculation of specimen's resistance.

4.3 Comparison of numerical and test results

The numerical analysis program is used to simulate the mechanical behavior of stiffened T-shaped CFST specimens. Concentric load - shortening relationship curves of TA specimens and eccentric load - mid-span horizontal displacement relationship curves of TE specimens are calculated to be compared with test results in Figure 19. Good agreement in stiffness, peak resistance and ductility guarantees the accuracy of the numerical program. The numerical program can be employed to predict stiffened T-shaped CFST specimens' mechanical behavior.

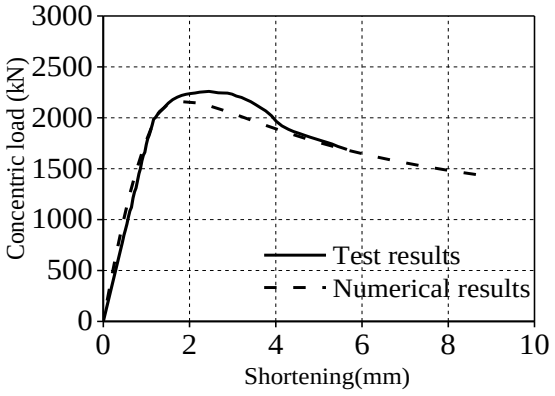

(a) TA3

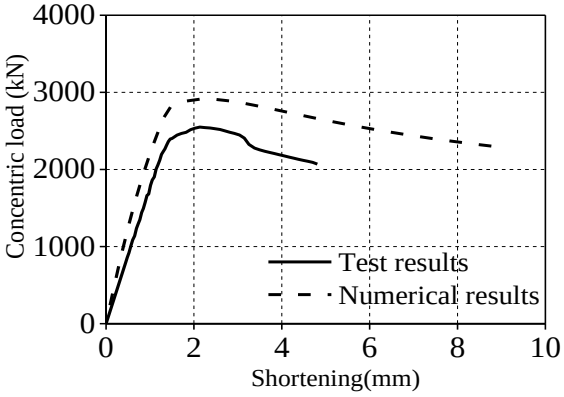

(b) TA4

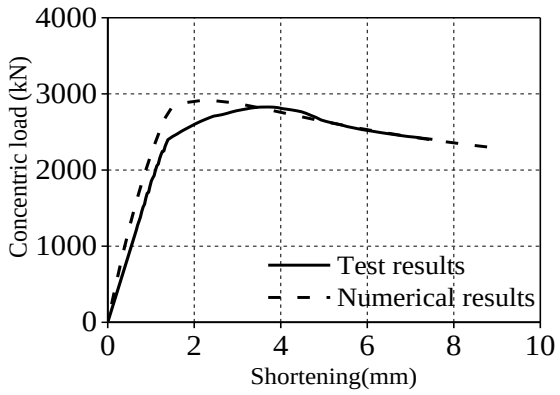

(c) TA5

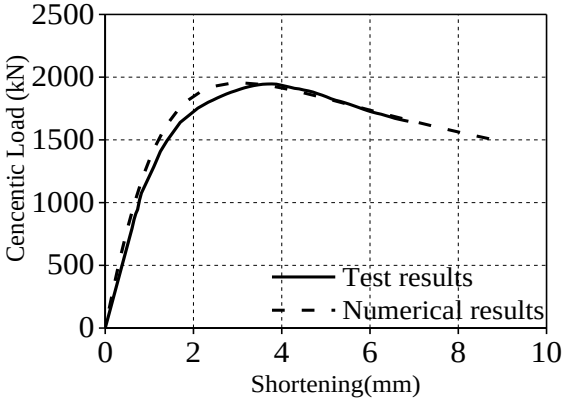

(d) TA7

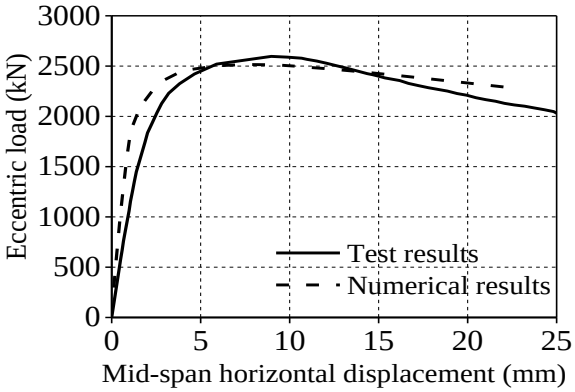

(e) TE3

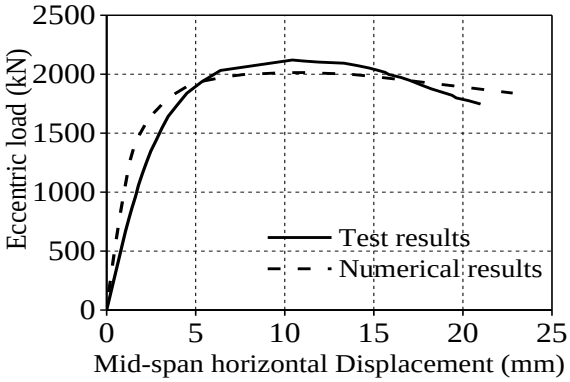

(f) TE4

Fig.19 Comparison of experimental and theoretical curves

5. Conclusions

(1) The tensile bar stiffeners effectively postpone the local buckling of T-shaped steel tube, increase the buckling resistance and upgrade classification of composite sections from Class 4 to Class 2 in Euro code 4. The tensile bar stiffened steel tube can provide more confinement for concrete, improve concrete failure mode and increase concrete compressive strength.

(2) For steel tube confined concrete specimen, the concave corners should be restricted with stiffeners to avoid concrete premature brittle failure.

(3) For specimens in TA group, the tensile bar stiffened T-shaped CFST specimen TA5 is provided with good mechanical behavior. Its ultimate resistance is 39% higher than that of the RC specimen TA1; its ductility is 93% higher than that of the non-stiffened specimen TA2. For specimens in TE group, the T-shaped CFST specimen TE4 stiffened by tensile bars has an increase in the peak resistance by 22% and ductility factor by 129% compared with RC specimen TE1. With the increase of eccentricity, the tensile bar stiffened T-shaped CFST specimen has a decrease in peak resistance by 18% and ductility factor by 32%.

(4) A numerical modeling program was developed incorporating the effect of the stiffeners on postponing of steel tube's local buckling and the confinement of steel tube for concrete. The

program was verified with related experimental data and good accuracy was achieved, therefore it can be used to predict the mechanical behavior of stiffened T-shaped CFST columns subjected to concentric and eccentric compressive load.

Acknowledgements

The project is supported by National Natural Science Foundation of China (51208241) and by Fundamental Research Funds for the Central Universities (lzujbky-2013-m01).

Reference

Cai, J. and He, Z.Q. (2005). "Axial load behavior of square CFT stub column with binding bars." *Journal of Constructional Steel Research*, 62, pp. 472-483.

Chen, Z.Y. (2003). "Construction techniques of concrete-filled rectangular steel tube (CFRT) columns and axial bearing capacity of concrete-filled special-shaped steel tube stubs." *Dissertation for the Master's Degree in Engineering*, Tongji Univercity. (in Chinese)

Cheng, T. and Thomas, Hsu. (1989). "T-shaped reinforced concrete members under biaxial bending and axial compression." *ACI Structural Journal*, 86(4), pp. 2576-2595.

Dundar, C. and Sahin, B. (1993). "Arbitrarily shaped reinforced concrete members subjected to biaxial bending and axial load." *Computer &Structures* , 49 (4), pp. 643-662.

Elremaily A and Azizinamini A. (2002). "Behavior and strength of circular concrete-filled tube columns." *Journal of Constructional Steel Research*, 58 (12), pp. 1567-1591.

Gao, D.X., Ke, J. and Wang, L.H. (2005). "Seismic behavior analysis of special-shaped column frame structure." *Journal of Xi'an University of Technology*, 21 (3), pp. 285-288. (in Chinese)

Joaquin, M. (1979). "Design aids for L-shaped reinforced concrete columns." *ACI Structural Journal*, 76(49), pp. 1197-1216.

Mallikarjuna and Mahadevappa, P. (1992). "Computer aided analysis of reinforced concrete columns subjected to axial compression and bending — I L-shaped sections." *Computer & Structures* , 44(5), pp. 121-1138.

Mander, J.B., Priestley, M.J.N. and Park, R. (1988). "Theoretical stress-strain model for confined concrete", *Journal of structural engineering*, 114(8), pp. 1804-1826.

Tao, Z., Han, L.H. and Wang, Z.B. (2005), "Experimental behaviors of stiffened concrete-filled thin-walled hollow steel structural (HSS) stub columns", *Journal of Constructional Steel Research*, 61, pp. 962-983.

Wang, D. and Lv, X.L. (2005). "Experimental study on seismic behavior of concrete-filled steel T-section and L-section columns." *Journal of Building Structures*, 26(4), pp. 39-44,106. (in Chinese)

Wang, T.C., Li, X.H., Wang, T.Z. and Kang, G.Y. (2007). "Hysteretic behavior of frame with specially shaped columns subjected to cyclic loading." *Journal of Jilin University (Engineering and Technology Edition)*, 37(1), pp. 224-228. (in Chinese)

Wang, Y.Y., Yang, Y.L., Zhang, S.M. and Liu, J.P. (2009). "Seismic behaviors of concrete-filled T-shaped steel tube columns." *Key Engineering Materials*, 400-402, pp. 667-683.

Yang Y.L., Yang H. and Zhang S.M. (2010). "Compressive behavior of T-shaped concrete filled steel tubular columns." *International Journal of Steel Structures*, 10(4), pp. 419-430.

Yang Y.L., Wang Y.Y. and Fu F. (2014). "Effect of reinforcement stiffeners on square concrete-filled steel tubular columns subjected to axial compressive load." *Thin-Walled Structures*, 82, pp. 132-144.

Yau, C.Y., Chan, S.L. and So, A.K.W. (1993). "Biaxial bending design of arbitrarily shaped reinforced concrete column." *ACI Structural Journal*, 90(3), pp. 269-279.

Zhang, D. and Ye, X.G. (2003). "Non-linear analysis of special-shaped reinforced concrete columns." *Journal of Hefei University of Technology*, 26(4), pp. 490-494. (in Chinese)

Zhang J.C., Shen Z.Y., Lin Z.Y. and Luo J.H. (2010). "Experimental research on seismic behavior of concrete-filled L-shaped steel tubular frames." *Journal of Building Structures*, 31(8), pp. 1-7. (in Chinese)

Zuo Z.L., Cai J., Yang C., Chen Q.J. and Sun G. (2012a). "Axial load behavior of L-shaped CFT stub columns with binding bars." *Engineering Structures*, 37, pp. 88-98.

Zuo Z.L., Cai J., Yang C. and Chen Q.J. (2012b). "Eccentric load behavior of L-shaped CFT stub columns with binding bars." *Journal of Constructional Steel Research*, 72, pp. 105-118.